High-Performance Supercapacitor Electrode Materials Prepared from Various Pollens

*Long Zhang, Fan Zhang, Xi Yang, Kai Leng, Yi Huang, and Yongsheng Chen**

High-performance supercapacitor electrode materials are prepared from biomass waste of various pollens at large scale through a green and low-cost chemical activation method. For example, the product prepared from lotus pollen exhibits ultrahigh specific surface area up to 3037 m^2 g^{-1} and large pore volume of 2.27 cm^3 g^{-1}, in which above 82% pore volume is contributed by the mesopores. Symmetric supercapacitor based on the product from lotus pollen shows high capacitance performance of 207 F g^{-1} at the current density of 1 A g^{-1} for neat $EMIMBF_4$ electrolyte. The corresponding gravimetric energy density is about ~88 Wh kg^{-1}, which is about 160% higher than that of commercial activated carbon (AC) RP20. And the volumetric energy density is ~44 Wh $liter^{-1}$, which is also larger than RP20 and graphene-based supercapacitors. Good rate performance is also achieved due to the abundant mesopores. Compared with the traditional ACs and graphene materials, the much better supercapacitor performance in liquid ionic (IL) system combined with the advantages of cheap carbon sources, green method and facile process should lead to the development of high performance supercapacitors in practical applications.

Carbon-based electrical double layer capacitors (EDLCs) or supercapacitors,[1,2] due to their unique properties of fast charging speed, high operational current, superior performance in extreme temperature and long cycle life,[2–4] have attracted tremendous attention in the past few years and already been widely applied in many practical areas such as hybrid electric vehicle, regenerative energy, emergency lighting and laser weapon.[5,6] However, the much lower energy density (~6 Wh kg^{-1}) of commercially available carbon-based supercapacitor has significantly limited its application for primary power source.[4,5] The energy stored in the carbon-based supercapacitor is proportional to its capacitance and the square of its operating voltage.[5,7] And the capacitance of the supercapacitor is primarily dependent on the effective specific surface area (SSA) of electrode materials while the operating voltage is determined by the electrolytes/solvents.[2,5,7,8] However, the commercially available ACs not only have poor SSA (<2000 m^2 g^{-1}), but also the pore size is so small (mainly below 0.6 nm)[9] that the ions of IL electrolytes can't access.[10] These will both lead to limited effective SSA of electrode materials in IL electrolytes which can offer high operating voltage. Furthermore, for the preparation of commercial ACs, some valuable materials such as coal, pitch and phenolic resin[1] are used as carbon sources and there is a significant carbon/material weight loss and serious toxic material releasing during the high temperature carbonization step, which caused waste of resources and environmental issues.

By viewing these, lot of efforts have been devoted on the preparation of ACs with high SSA and matched pore size in economical and environmentally friendly ways. Some cheap carbon sources such as seaweed and a series of starch were used as raw materials for ACs and good capacitance performance was achieved in the aqueous electrolytes.[11,12] But the energy density still needs to be improved by further increasing SSA and operating voltage of electrolytes. Hydrothermal carbonization which could largely reduce the materials waste and releasing of toxic chemicals has been widely considered and used to replace the high temperature carbonization.[13–15] The products from combined process of hydrothermal carbonization and chemical activation exhibited high SSA and excellent capacitance performance in the organic electrolytes.[8] However, the small pore size of these resulting products still limited their application in the ILs, which have larger ion size but can supply higher operating voltage. Meanwhile, some new carbon materials such as carbon nanotube (CNT) and graphene were also used as electrode materials for supercapacitor application. The achieved gravimetric specific capacitance and gravimetric energy density in IL electrolytes are fascinating.[16,17] However, the density of these CNT or graphene electrodes are relatively lower (~0.3 g cm^{-3}) than commercial AC electrodes (~0.5 g cm^{-3}),[1] resulting in actually the same or lower volumetric energy density than commercial ACs. Therefore, it is still highly demanded for cheap AC electrodes with large SSA, matched pore size and moderate density to achieve the high energy density of supercapacitor.[8]

As potential carbon sources, pollens are common biomass waste which are very cheap and also widely available. And

L. Zhang, F. Zhang, X. Yang, K. Leng,
Prof. Y. Huang, Prof. Y. Chen
Key Laboratory for Functional Polymer Materials and Centre for Nanoscale Science and Technology
Institute of Polymer Chemistry
College of Chemistry Nankai University
Tianjin, 300071, China
E-mail: yschen99@nankai.edu.cn

DOI: 10.1002/smll.201202943

© 2013 Wiley-VCH Verlag GmbH & Co. KGaA, Weinheim

more importantly, most pollens have unique porous surface structure, which can help them fully mix and react with activating agents such as potassium hydroxide (KOH), zinc chloride or sodium hydroxide to achieve high SSA and enlarge the pore size.[18] Furthermore, similar to many ACs prepared from natural carbon sources such as cellulose or coconut shells, ACs prepared from pollens should have higher density than CNT and graphene. Thus, pollens are promising candidates for carbon sources of ACs.

Based on these unique properties of pollens and considering the environmental issues, in this work, various pollens with porous surface structure were studied as carbon sources and treated by hydrothermal carbonization and further industrial chemical activation. All the products showed much higher Brunauer-Emmett-Teller (BET) SSA (>2600 m^2 g^{-1}) than the commercial compared sample AC of RP20 (1677 m^2 g^{-1}), and the pores in the products were mainly mesopores, which is larger than that of RP20 and matched much better for the application in organic electrolytes or ILs with large ion size and high viscosity. The electrode density of our materials is about 0.5 g cm^{-3}, which is close to that of commercial ACs and higher than CNT or graphene. The performance of symmetric supercapacitors based on the products was determined by the most recommended method/standard[19] and compared with RP20 and other reported carbon materials, which exhibited high specific capacitance and energy density and good rate performance in both the most common organic electrolyte of 1 M tetraethylammonium tetrafluoroborate in AN ($TEABF_4$/AN) and 1-Ethyl-3-methylimidazolium tetrafluoroborate ($EMIMBF_4$).

Details for preparation of ACs from various pollens were shown in the experimental sections. For hydrothermal carbonization, the aqueous suspension of each kind of pollens was transferred to sealed Teflon-lined autoclaves and maintained at 180 °C for 12 h. The products of hydrothermal carbonization were denoted as lotus-H, peony-H, rape-H and camellia-H, respectively. Then the hydrothermal product was fully mixed with 4 times weight KOH and activated in a horizontal tube furnace at 900 °C for 1 h under Ar. The resulting solid was washed and dried to get the final products, which were denoted as lotus-HA, peony-HA, rape-HA and camellia-HA, respectively.

The structure and morphology of hydrothermal products and final products prepared from various pollens were analyzed by scanning electron microscopy (SEM). From Supporting Information (SI) Figure S1a-d, we can see that after hydrothermal step the macro scale structure/shape and porous structures remain as before. Different from the traditional carbon source such as phenolic resin for preparation of AC, the porous structure in hydrothermal products of pollens make them much easier to mix and react with KOH, which may lead to a much higher SSA than the traditional ACs. After the activation step, all the products showed solid structure with irregular shape and lateral size of 10–20 µm (Figure S1e–h). This is very different from the 3D network in pure graphene electrodes as reported in some literatures, which may have over much empty space and result in rather low density.[20]

Elemental analysis was performed to determine the elemental composition of the products. SI, Table S1 shows that all our products consist of ~92–95 wt% of carbon, ~1.4–2.0 wt% H, and ~3–6 wt% O, which is similar to that of RP20. This suggests that our products are carbon-based materials with very few percent of hydrogen or oxygen containing groups. Raman is a powerful tool to provide structural and quality characterization of the carbon-based materials. The typical Raman spectra of the products is shown in SI, Figure S2 and compared with RP20. Similar with the Raman spectra of ACs reported in previous literature[21] and RP20, our products showed the G-band located around 1600 cm^{-1} which belongs to graphite in-plane vibrations[22] and the broad and strong peak located around 1350 cm^{-1} which should be attributed to the disorder-induced D band,[22,23] also indicating that our products are carbon-based materials. And the relatively lower value of I_D/I_G in our products than RP20 suggest a lower content of sp^3 carbon and better quality of our materials than RP20.[21,24–26]

In order to study the SSA and distribution of pore volume in the products, N_2 adsorption/desorption isotherms were tested and compared with RP20. The detailed SSA and pore volume distribution of all the products are listed in **Table 1**. The BET SSA is calculated in the linear relative pressure range from 0.05 to 0.3 in **Figure 1**a. All the products show large BET SSA above 2673 m^2 g^{-1} and the highest BET SSA reaches 3037 m^2 g^{-1} for lotus-HA, which is much higher than that of RP20 (1677 m^2 g^{-1}). This is because the porous structure in hydrothermal products of pollens makes them much easier to mix and react with KOH, which leads to a much higher SSA than the traditional AC like RP20. XRD characterization also suggests that our products have much weaker and broader (002) peak than RP20 (SI, Figure S3), indicating a more disturbed structure due to the more randomly oriented aromatic carbon sheets in the amorphous carbon,[25,27] which is beneficial for higher SSA. The typical hysteresis loop (Figure 1a) between the adsorption and desorption branches in our products is associated with capillary condensation taking place in mesopores and given by many mesoporous industrial adsorbents, indicating the existence of many mesopores in the products.[28] In the contrast, RP20 showed no hysteresis loop, which is characteristic for microporous materials.[8] As a typical example of our products, the cumulative pore volume and distribution of pore volume in lotus-HA was shown in Figure 1b, which exhibited

Table 1. BET SSA and distribution of pore volume in all the products, with RP20 for comparison.

Products	BET SSA [m^2 g^{-1}]	pore volume [cm^3 g^{-1}]	pore volume (micropore) [cm^3 g^{-1}]	pore volume (mesopore) [cm^3 g^{-1}]
lotus-HA	3037	2.27	0.41	1.86
peony-HA	2673	1.50	0.48	1.02
rape-HA	2765	2.20	0.41	1.79
camellia-HA	2819	2.06	0.45	1.62
RP20	1677	0.64	0.60	0.04

© 2013 Wiley-VCH Verlag GmbH & Co. KGaA, Weinheim
small 2013,
DOI: 10.1002/smll.201202943

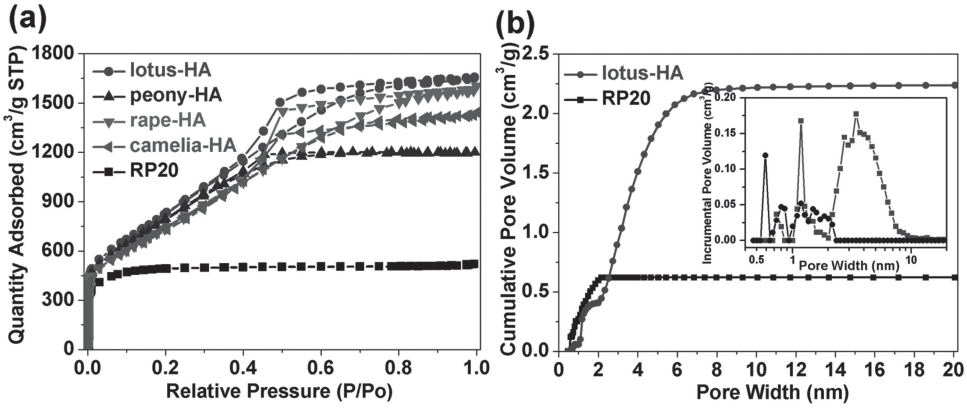

Figure 1. a) N_2 adsorption/desorption analysis of our products and RP20. Product lotus-HA shows highest BET SSA values up to 3037 m^2 g^{-1} (calculated in the linear relative pressure range from 0.05 to 0.3) and the typical hysteresis loop between the adsorption and desorption branches indicates the existence of many mesopores in the products. b) Cumulative pore volume and (inset) distribution of pore volume for N_2 (calculated using a slit/cylindrical non-local density functional theory model). Product lotus-HA has a huge pore volume of 2.27 cm^3 g^{-1} and above 82% pore volume is contributed by the mesopores.

a huge pore volume of 2.27 cm^3 g^{-1} and above 82% pore volume is contributed by the mesopores, while RP20 showed much smaller pore volume of 0.64 cm^3 g^{-1} and only 6% pore volume is contributed by the mesopores. We believe that the introduction of many mesopores also can be ascribed to the unique porous structure of pollens. Previous study has demonstrated the preparation of microporous ACs with high SSA (>2400 m^2 g^{-1}) and large pore volume of 1.08 cm^3 g^{-1} (only 13% pore volume is contributed by the mesopores) by treating cellulose or starch through the same hydrothermal carbonization and chemical activation method.[8] Compared with the solid carbonaceous spheres structure in the hydrothermal products of cellulose and starch,[15] the unique porous structure in the hydrothermal products of pollens make KOH much easier to penetrate into the produced micropores so that many mesopores can be formed by further activation process of micropores, including pore widening, fusing and wall collapsing.[18]

The high SSA and mesoporous property of our products make them good candidates for electrode materials of supercapacitors, especially for supercapacitors based on organic electrolytes and ILs which can supply high operating voltage (high energy density) but have large ion size and high viscosity.[29] Symmetric supercapacitors based on the products from pollens have been fabricated and tested by the most recommended method and compared with RP20.[19,30] Both the most popular organic electrolyte of 1 M $TEABF_4$/AN and IL of $EMIMBF_4$ were used as the electrolytes. All the products give similar but excellent supercapacitor performance, with the best results from the product lotus-HA which gives a specific capacitance of 185 F g^{-1} in 1 M $TEABF_4$/AN and 207 F g^{-1} in neat $EMIMBF_4$ electrolytes, respectively, at the current density of 1 A g^{-1}, while those are just 110 F g^{-1} and 130 F g^{-1} for RP20. The galvanostatic charge/discharge curves of the supercapacitors based on product lotus-HA in 1 M $TEABF_4$/AN and IL electrolytes are shown in **Figure 2**a,b. For the devices based on product lotus-HA measured at the current density of 1 A g^{-1}, the corresponding gravimetric energy densities are as high as 46 Wh kg^{-1} in 1 M $TEABF_4$/AN and 88 Wh kg^{-1} for neat $EMIMBF_4$ electrolyte, respectively, based on the weight of electrode materials. The capacitance performance of ACs from various pollens were summarized in **Figure 3** and compared with RP20 and other carbon materials reported in literatures.[8,11,16,17,20,29,31,32] We can see that due to high SSA and mesoporous property, ACs from various pollens can achieved excellent specific capacitance in IL electrolyte which can supply much higher operating voltage than aqueous and organic electrolytes, leading to a much higher gravimetric energy density than RP20 and other reported carbon materials.

Recently it has been demonstrated that due to the density difference of various carbon based electrodes, it is more recommended to use volumetric energy density to evaluate the carbon based electrode materials for supercapacitor application.[30] The densities of electrodes based on our products are ~0.5 g cm^{-3}, which is close to that of RP20 (~0.6 g cm^{-3}) and higher than that of graphene materials (~0.3 g cm^{-3}).[1] Therefore, the volumetric energy density of ~44 Wh $liter^{-1}$ for lotus-HA electrode in neat $EMIMBF_4$ electrolyte is higher than that (~33 Wh $liter^{-1}$) of RP20. And for some reported graphene electrodes, although a high gravimetric energy density of 85 Wh kg^{-1} can be achieved for the electrode materials, its volumetric energy density is just ~26 Wh $liter^{-1}$ due to the low density of graphene electrode (0.3 g cm^{-3}), which is much smaller than the value of RP20 and our products.[30] Furthermore, compared with graphene, the ACs from pollens are much more economical electrode materials for the large scale application in the supercapacitor, since the pollens are very cheap and the preparation process is quite simple and green.

Supercapacitors based on ACs from pollens exhibited good cycle stability. For example, the supercapacitor devices based on lotus-HA still keep ~96% capacitance in 1 M $TEABF_4$/AN and ~95% in $EMIMBF_4$ electrolytes after 5000 times of charging/recharging at the current density of 1 A/g (SI, Figure S4). Supercapacitors based on our products also showed good capacitance performance at high current density of 10 A/g, indicating a good rate performance

DOI: 10.1002/smll.201202943
© 2013 Wiley-VCH Verlag GmbH & Co. KGaA, Weinheim

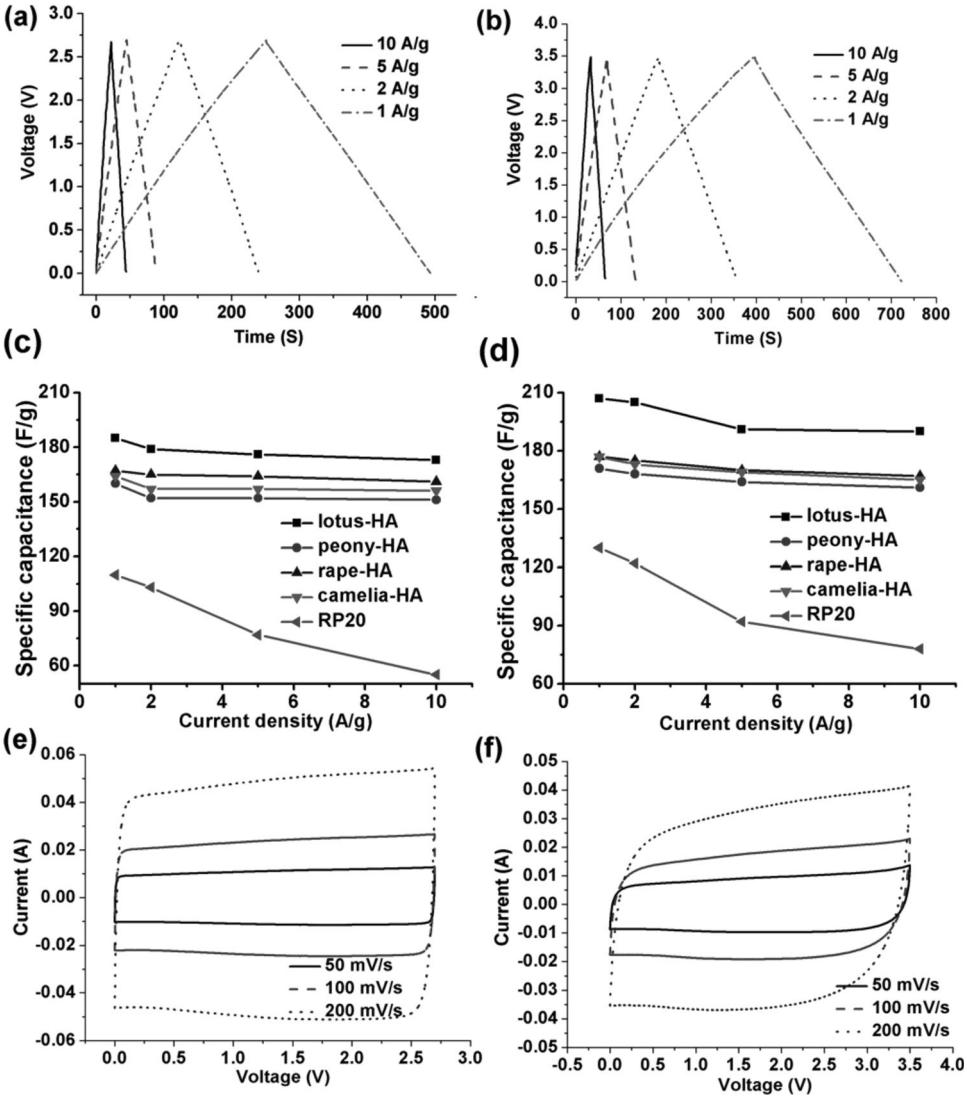

Figure 2. Galvanostatic charge/discharge curves of lotus-HA based supercapacitors in a) 1 M $TEABF_4$/AN and b) neat $EMIMBF_4$ electrolytes under different constant currents. Rate performance of supercapacitors based on our products and RP20 in c) 1 M $TEABF_4$/AN and d) neat $EMIMBF_4$ electrolyte under different constant currents. Supercapacitors based on our products show good capacitance performance at high current density, indicating a good rate performance and rapid ion transport characteristics. CV curves of lotus-HA based supercapacitors in e) 1 M $TEABF_4$/AN and f) neat $EMIMBF_4$ electrolytes under different scan rates, which exhibit good rectangular curves over a wide range of voltage scan rates (50–200 mV s^{-1}).

and rapid ion transport characteristics due to the abundant mesopores[33] (Figure 2c,d). In contrary, the specific capacitance of RP20 based supercapacitors was dramatically decreased with increasing current density. This is probably due to the relatively smaller pore size in RP20 so that large electrolyte ions can not fully and fast access at the high current density.[4] Cyclic voltammetry (CV) and electrical impedance spectroscopy (EIS) characterization were also performed to study the rate performance. The CV curves of lotus-HA based supercapacitors under different scan rates in 1 M $TEABF_4$/AN and neat $EMIMBF_4$ electrolytes exhibited good rectangular curves over a wide range of voltage scan rates (50–200 mV s^{-1}), indicating a good rate performance (Figure 2e,f).[34] In the contrast, the distorted rectangular shapes in the CV curves of RP20 based supercapacitors under different scan rates in 1 M $TEABF_4$/AN and neat $EMIMBF_4$ electrolytes indicate poor rate performance (SI, Figure S5). And from the EIS results in SI, Figure S6, not only our products have a relatively low equivalent series resistance (the corresponding value of the intercept on the X axis) than RP20,[35] but also they showed the much shorter Warburg region portion (the slope of the 45° portion of the curve) than RP20 for better ion diffusion efficiency.[36]

In summary, using biomass waste of various pollens, high-performance supercapacitor electrode materials with high SSA, mainly mesoscale pores and high density through a green and low-cost chemical activation method were developed. Compared with traditional carbon sources for ACs, the porous surface structure of pollens offer better activation access for higher SSA and more mesopore structure. The combined superior properties make these materials exhibit excellent specific capacitance and high energy density for

© 2013 Wiley-VCH Verlag GmbH & Co. KGaA, Weinheim
small 2013,
DOI: 10.1002/smll.201202943

small

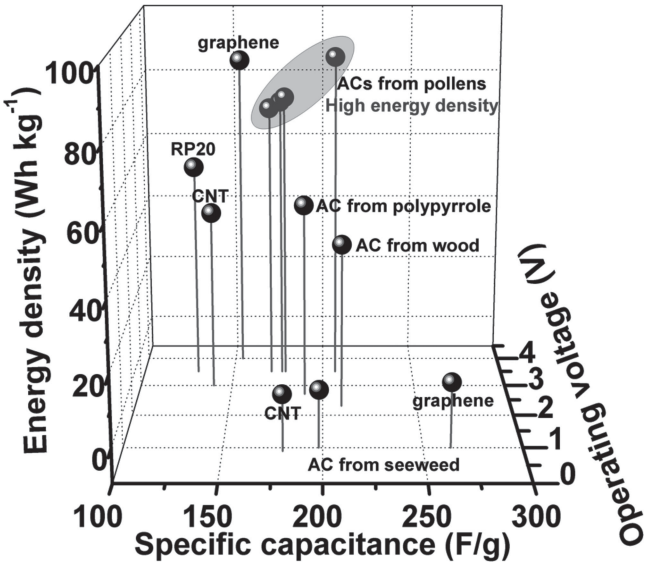

Figure 3. Summary of capacitance performance of ACs from pollens, with RP20 and other carbon materials reported in literatures for comparison. The specific capacitance of different carbon materials were compared at the same charge/discharge current density of 1 A/g. ACs from various pollens can achieved much higher gravimetric energy density than RP20 and other reported carbon materials.

supercapacitors in IL electrolytes, which is about 160% larger than the commercial AC of RP20. And the volumetric energy density is also larger than graphene based supercapacitors due to the higher density than graphene electrodes. These results, together with the advantages of cheap carbon sources, green method and facile process will hold great promise for high performance supercapacitors in practical applications.

Experimental Section

Materials: Various pollens from lotus, peony, rape and camellia were purchased from commercial available products. Potassium hydroxide (KOH, Wuhan Chujiang Chemical Co., Ltd.) was used without further treatment. Poly(tetrafluoroethylene) (PTFE, solid powder, Dupont), commercial activated carbon RP20 (Kuraray Chemicals) and electrolytes including 1 M tetraethylammonium tetrafluoroborate in AN ($TEABF_4$/AN, Novolyte), 1-ethyl-3-methylimidazolium tetrafluoroborate ($EMIMBF_4$, Novolyte) were all used as purchased. The cellulose film (TF4840, NKK) were used as separator for supercapacitor.

Preparation of AC with High Surface Area from Various Pollens: The preparation of ACs from various pollens includes a hydrothermal process and followed by an industry KOH activation step. Briefly, for each kind of pollens, 16 g pollen were added into 80 ml water and stirred for 1 h to form homogeneous suspension. The as-prepared suspension was then transferred to a sealed 100 mL Teflon-lined autoclave heated up to 180 °C and maintained at this temperature for 12 h. The resulting solid product was then filtered, washed three times and dried in vacuum at 120 °C for 24 h. The products of hydrothermal carbonization were denoted as lotus-H, peony-H, rape-H and camellia-H, respectively. Then the hydrothermal product was fully mixed with 4 times weight KOH, then placed in a horizontal tube furnace and heated from room temperature to 900 °C for 1 h at 5 °C min^{-1} under Ar. The resulting product was thoroughly washed with 0.1 M HCl to remove any inorganic salts, then washed with distilled water until the pH value reached 7 and finally dried in vacuum at 120 °C for 24 h. The final products prepared from various pollens were denoted as lotus-HA, peony-HA, rape-HA and camellia-HA, where the suffix "H" and "A" represented the hydrothermal carbonization and activation process, respectively. Commercial AC RP20 was used as a control material.

Characterization: The morphology of various raw pollens and their final products were analyzed by scanning electron microscopy using LEO 1530 VP field emission scanning electron microscope with acceleration voltage of 10 kV. X-ray diffraction measurements were performed on a Rigaku D/Max-2500 diffractometer with Cu Kα radiation. Raman spectra were examined with a LabRAM HR Raman spectrometer using laser excitation at 514.5 nm. Lorentzian fitting was carried out to obtain the positions and widths of the D and G bands in the Raman spectra. I_D and I_G are the intensities of the D and G bands, respectively. The nitrogen adsorption/desorption analysis was done at 77 K on a Micromeritics ASAP 2020 apparatus. The SSA was calculated by the BET method based on adsorption data in the relative pressure (P/P_0) range of 0.05 to 0.3. The total pore volume was measured from the amount of nitrogen adsorbed at a relative pressure (P/P_0) of 0.99. The distribution of pore volume was analyzed using a NL-DFT method with a slit pore model from the nitrogen adsorption data.

Fabrication of Supercapacitors and their Performance Evaluation: The industry-level two-electrode symmetric supercapacitors based on our materials were fabricated to determine the capacitance performance. Briefly, 90 wt% products and 10 wt% PTFE were homogeneously mixed in the agate mortar. Then the mixture was rolled into 100–120 μm thickness sheets and punched into 16 mm diameter electrodes. After dried at 120 °C for 6 h under vacuum, the electrodes were weighted and hot pressed onto the current collectors (aluminum foils with conducting carbon coating) and then dried at 180 °C for 6 h under high vacuum to completely remove water. The mass and thickness of electrode films are 9.2–10.8 mg and 90–110 μm so that the calculated densities of electrode films are about 0.5 g cm^{-3}. The dry electrodes/collectors were transferred into a glove box filled with Ar to construct two-electrode symmetrical supercapacitors, which consisted of two current collectors, two electrodes with identical weight and a porous cellulose separator sandwiched in a test fixture consisting of two stainless steel plates. 1 M $TEABF_4$/AN and $EMIMBF_4$ were used as electrolytes, respectively. All the electrochemical tests were carried out at room temperature. Galvanostatic charge-discharge cycle tests were measured using an Arbin testing system (Arbin MSTAT, America) at current densities of 1, 2, 5 and 10 A g^{-1}, respectively. The gravimetric specific capacitance, C_s (F g^{-1}), was calculated according to

$$C_s = \frac{4I}{mdV/dt}$$

where I is the constant current (A), m is the total mass of two electrodes (g) and dV/dt (V s^{-1}) is the slope obtained by fitting a straight line to the discharge curve over the range of V (the voltage at the beginning of discharge) to ½ V. The energy density, E_{cell} (Wh kg^{-1}), was estimated using the formula $E_{cell} = C_s V^2/8$. CV and

DOI: 10.1002/smll.201202943
© 2013 Wiley-VCH Verlag GmbH & Co. KGaA, Weinheim

EIS studies were performed using Autolab (Metrohm). CV tests were carried out in various scan rates ranging from 50 mV s^{-1} to 200 mV s^{-1}. The applied voltage windows are differed from different electrolytes, which was 0–2.7 V for 1 M $TEABF_4$/AN electrolyte and 0–3.5 V for $EMIMBF_4$. EIS measurements were carried out at an AC amplitude 10 mV in the range of from 100 kHz to 10 mHz.

Supporting Information

Supporting Information is available from the Wiley Online Library or from the author.

Acknowledgements

The authors gratefully acknowledge financial support from the MOST (Grants 2012CB933401 and 2011CB932602) and NSFC (Grants 51273093, 50902073, 50903044 and 50933003).

[1] P. Simon, Y. Gogotsi, *Acc. Chem. Res.* **2012**.
[2] A. Ghosh, Y. H. Lee, *ChemSusChem* **2012**, *5*, 480–499.
[3] Y. Zhai, Y. Dou, D. Zhao, P. F. Fulvio, R. T. Mayes, S. Dai, *Adv. Mater.* **2011**, *23*, 4828–4850.
[4] E. Frackowiak, *Phys. Chem. Chem. Phys.* **2007**, *9*, 1774–1785.
[5] P. Simon, Y. Gogotsi, *Nat. Mater.* **2008**, *7*, 845–854.
[6] A. Burke, *Int. J. Energy Res.* **2010**, *34*, 133–151.
[7] P. J. Hall, M. Mirzaeian, S. I. Fletcher, F. B. Sillars, A. J. R. Rennie, G. Shitta-Bey, G. Wilson, A. Cruden, R. Carter, *Energy Environ. Sci.* **2010**, *3*, 1238–1251.
[8] L. Wei, M. Sevilla, A. B. Fuertes, R. Mokaya, G. Yushin, *Adv. Energy Mater.* **2011**, *1*, 356–361.
[9] S. Inagaki, K. Oikawa, Y. Kubota, *Chem. Lett.* **2009**, *38*, 918–919.
[10] C. Largeot, C. Portet, J. Chmiola, P. L. Taberna, Y. Gogotsi, P. Simon, *J. Am. Chem. Soc.* **2008**, *130*, 2730–2731.
[11] E. Raymundo-Pinero, F. Leroux, F. Beguin, *Adv. Mater.* **2006**, *18*, 1877–1882.
[12] Q. Y. Li, H. Q. Wang, Q. F. Dai, J. H. Yang, Y. L. Zhong, *Solid State Ionics* **2008**, *179*, 269–273.
[13] E. Berl, A. Schmidt, *Justus Liebigs Ann. Chem.* **1932**, *493*, 97–123.
[14] M. M. Titirici, M. Antonietti, N. Baccile, *Green Chem.* **2008**, *10*, 1204–1212.
[15] B. Hu, K. Wang, L. Wu, S. H. Yu, M. Antonietti, M. M. Titirici, *Adv. Mater.* **2010**, *22*, 813–828.
[16] K. H. An, W. S. Kim, Y. S. Park, Y. C. Choi, S. M. Lee, D. C. Chung, D. J. Bae, S. C. Lim, Y. H. Lee, *Adv. Mater.* **2001**, *13*, 497.
[17] C. Liu, Z. Yu, D. Neff, A. Zhamu, B. Z. Jang, *Nano Lett.* **2010**, *10*, 4863–4868.
[18] N. Shiratori, K. Lee, J. Miyawaki, S. H. Hong, I. Mochida, B. An, K. Yokogawa, J. Jang, S. H. Yoon, *Langmuir* **2009**, *25*, 7631–7637.
[19] M. D. Stoller, R. S. Ruoff, *Energy Environ.Sci.* **2010**, *3*, 1294–1301.
[20] Y. Sun, Q. Wu, G. Shi, *Phys. Chem. Chem. Phys.* **2011**, *13*, 17249–17254.
[21] N. Shimodaira, A. Masui, *J. Appl. Phys.* **2002**, *92*, 902–909.
[22] R. J. Nemanich, S. A. Solin, *Phys. Rev. B* **1979**, *20*, 392–401.
[23] A. C. Ferrari, J. Robertson, *Philos. T. R. Soc. A.* **2004**, *362*, 2477–2512.
[24] A. Reina, X. Jia, J. Ho, D. Nezich, H. Son, V. Bulovic, M. S. Dresselhaus, J. Kong, *Nano Lett.* **2008**, *9*, 30–35.
[25] J. Zhao, L. Yang, F. Li, R. Yu, C. Jin, *Carbon* **2009**, *47*, 744–751.
[26] A. C. Ferrari, *Mater. Res. Soc. Symp. Proc.* **2001**, *675*, W11.5.1–12.
[27] A. Onda, T. Ochi, K. Yanagisawa, *Top Catal.* **2009**, *52*, 801–807.
[28] K. S. W. Sing, D. H. Everett, L. Moscou, R. Pierrotti, J. Roquerol, T. Siemeniewska, *Pure Appl. Chem.* **1985**, *57*, 603.
[29] L. Wei, M. Sevilla, A. B. Fuertes, R. Mokaya, G. Yushin, *Adv. Funct. Mater.* **2012**, *22*, 827–834.
[30] Y. Gogotsi, P. Simon, *Science* **2011**, *334*, 917–918.
[31] W. Lv, D. M. Tang, Y. B. He, C. H. You, Z. Q. Shi, X. C. Chen, C. M. Chen, P. X. Hou, C. Liu, Q. H. Yang, *ACS Nano* **2009**, *3*, 3730–3736.
[32] Z. Niu, W. Zhou, J. Chen, G. Feng, H. Li, W. Ma, J. Li, H. Dong, Y. Ren, D. Zhao, S. Xie, *Energy Environ. Sci.* **2011**, *4*, 1440–1446.
[33] M. Lazzari, M. Mastragostino, A. Pandolfo, V. Ruiz, F. Soavi, *J. Electrochem.Soc.* **2011**, *158*, A22–A25.
[34] K. Sheng, Y. Sun, C. Li, W. Yuan, G. Shi, *Sci. Rep.* **2012**, *2*, 247.
[35] B. G. Choi, J. Hong, W. H. Hong, P. T. Hammond, H. Park, *ACS Nano* **2011**, *5*, 7205–7213.
[36] Y. Wang, Z. Shi, Y. Huang, Y. Ma, C. Wang, M. Chen, Y. Chen, *J. Phys. Chem. C* **2009**, *113*, 13103–13107.

Received: November 27, 2012
Revised: January 8, 2013
Published online:

© 2013 Wiley-VCH Verlag GmbH & Co. KGaA, Weinheim

DOI: 10.1002/smll.201202943

Copyright WILEY-VCH Verlag GmbH & Co. KGaA, 69469 Weinheim, Germany, 2013.

NANO MICRO small

Supporting Information

for *Small*, DOI: 10.1002/smll.201202943

High-Performance Supercapacitor Electrode Materials Prepared from Various Pollens

*Long Zhang, Fan Zhang, Xi Yang, Kai Leng, Yi Huang, and Yongsheng Chen**

Supporting Information

High-performance supercapacitor electrode materials prepared from various pollens**

*Long Zhang, Fan Zhang, Xi Yang, Kai Leng, Yi Huang, Yongsheng Chen**

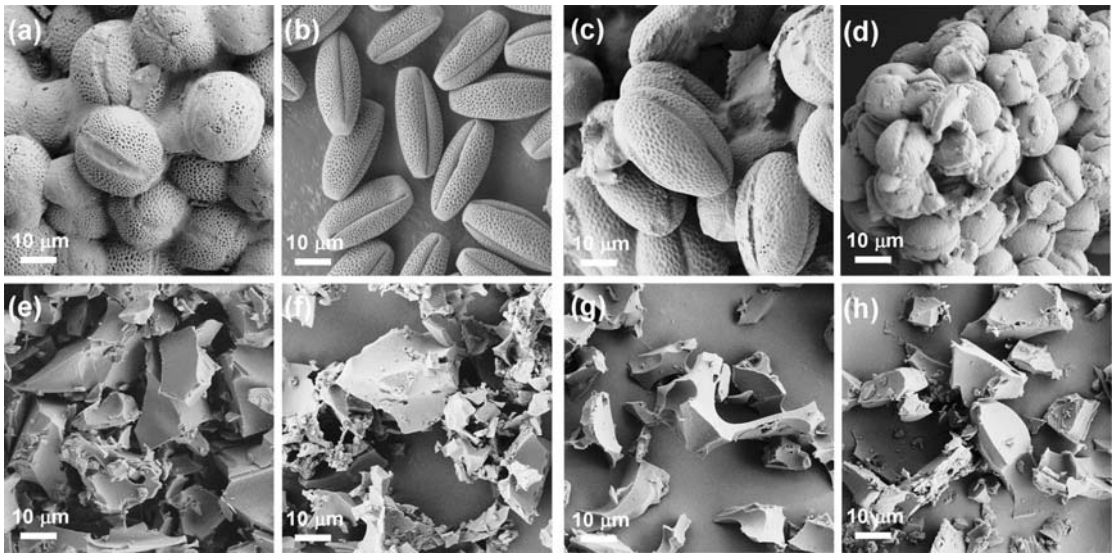

Figure S1. SEM images of the products from hydrothermal carbonization: a) lotus-H, b) peony-H, c) rape-H and d) camellia-H. All the hydrothermal products show porous or wrinkled surface structure. SEM images of the final products: e) lotus-HA, f) peony-HA, g) rape-HA and h) camellia-HA. Regardless of the carbon precursor, the products from different pollens all show irregular shape with a lateral size of 10-20 μm.

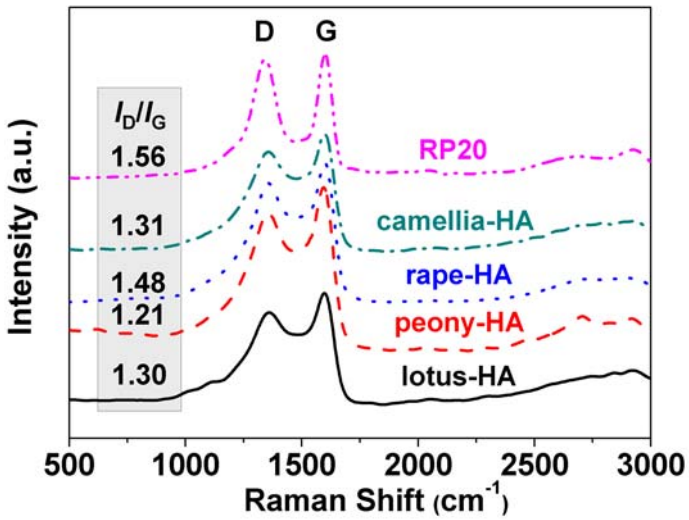

Figure S2. Raman spectra of the products and RP20, with I_D/I_G value calculated from the integral intensities of the D and G bands. The G-band located around 1600 cm^{-1} belongs to graphite in-plane vibrations and the broad and strong peak located around 1350 cm^{-1} is attributed to the disorder-induced D band, indicating that our products are carbon-based materials. Our products showed a relatively lower value of I_D/I_G than RP20, indicating a lower content of sp^3 carbon and better quality of our materials than RP20.

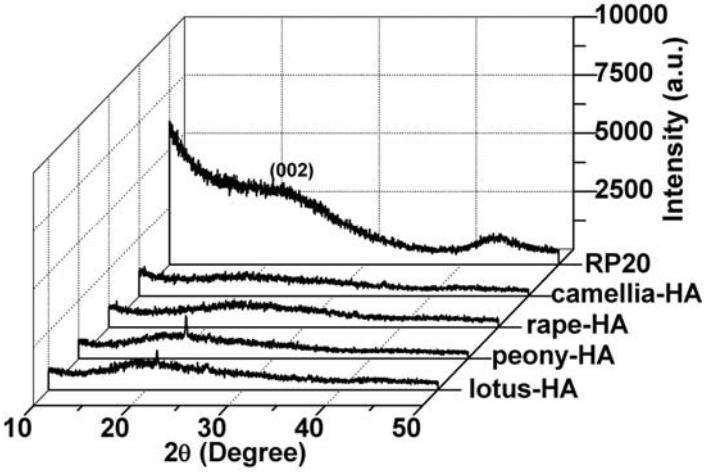

Figure S3. XRD curves of our products and RP20. Much weaker and broader (002) peaks were observed in our products than RP20, indicating a more disturbed structure in our products.

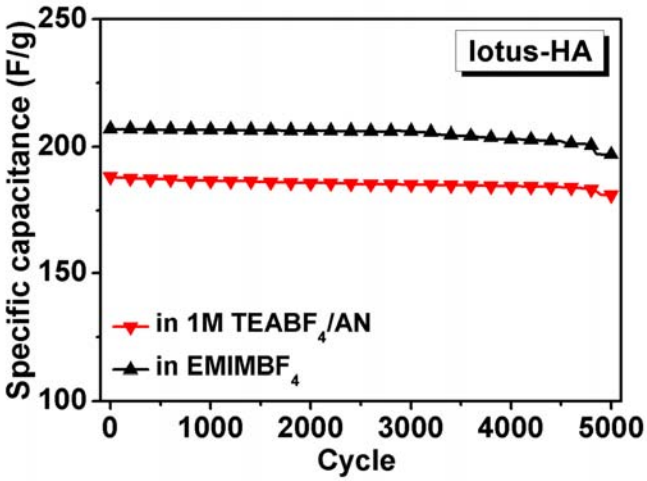

Figure S4. Cycle stability of lotus-HA based supercapacitor in two electrolytes. After 5000 times of charging/recharging, capacitance retention of ~96% in 1 M $TEABF_4$/AN and ~95% in $EMIMBF_4$ electrolytes was observed, respectively.

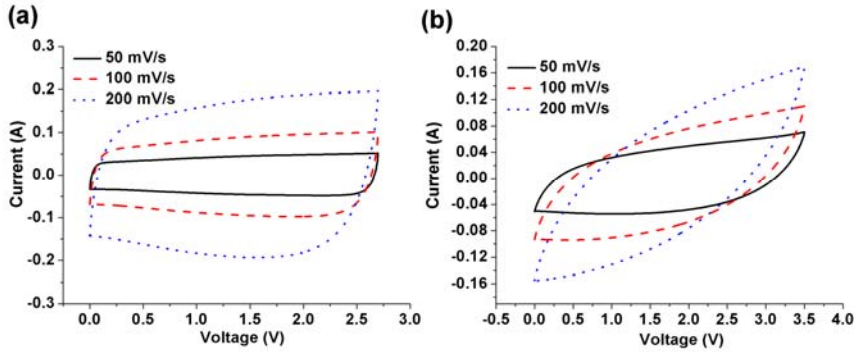

Figure S5. CV curves of RP20 based supercapacitor under different scan rates in a) 1 M $TEABF_4$/AN and b) neat $EMIMBF_4$ electrolytes. The distorted rectangular shapes indicate bad rate performance.

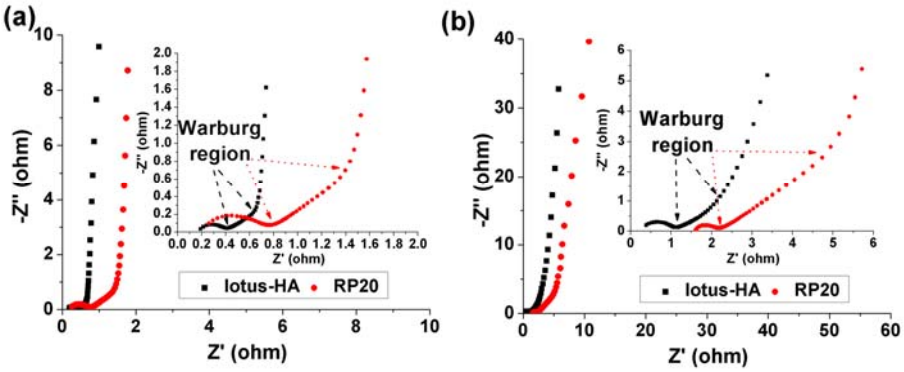

Figure S6. Electrical impedance spectroscopy of supercapacitors based on lotus-HA and RP20 in a) 1 M $TEABF_4$/AN and b) $EMIMBF_4$ electrolytes. Supercapacitors based on our products not only have a relatively low equivalent series resistance (the corresponding value of the intercept on the X axis) than RP20, but also they showed the much shorter Warburg region portion (the slope of the 45° portion of the curve) than RP20 for better ion diffusion efficiency.

Table S1. Elemental analysis of all the products, with commercial AC of RP20 for comparison. Our products are carbon-based materials with very few percent of hydrogen or oxygen containing groups.

Products	Weight percent (%)			Atomic ratio	
	C	H	O	C/H	C/O
lotus-HA	94.92	1.97	3.11	4	40.7
peony-HA	93.91	1.41	4.68	5.6	26.8
rape-HA	93.73	1.42	4.85	5.5	25.8
camellia-HA	91.67	1.89	6.44	4	19
RP20	93.67	1.7	4.63	4.6	27